JOURNAL OF SPACECRAFT AND ROCKETS
Vol. 45, No. 2, March–April 2008

Influence of Laminar Boundary-Layer Transition on Entry Vehicle Designs

T. C. Lin*
Northrop-Grumman Corporation, San Bernardino, California 92408

DOI: 10.2514/1.30047

A review of the influence of the laminar boundary-layer transition to turbulent-flow phenomenon upon a high-speed entry vehicle performance is made. In addition to the heating augmentation associated with the advent of transitional and turbulent boundary layers, attention is also focused on other aspects of vehicle performance parameters such as the unique flight dynamics associated with the boundary-layer transition altitude, aerodynamic stability degradation, lateral trim load increase, and potentially large vehicle impact dispersion. A remedy to alleviate these adverse effects induced by the boundary-layer transition phenomenon is proposed. This consists of entry vehicle configuration selection, thermal protection material tradeoffs, and flight trajectory optimization.

Nomenclature

A	=	reference area, m^2
B'	=	nondimensional wall ablation and blowing parameter, $\dot{m}/(\rho_e u_e Ch)$
C' C''	=	constants used in low-recession nosetip boundary-layer transition correlations ($\sim$110 and $\sim$250, respectively)
Ch	=	local heat-transfer coefficient including the wall blowing effects
C_L	=	lift coefficient
Cm, Cn, Cm_α	=	aerodynamic pitching moment, yaw moment, and pitching moment slope
Cm_q, $Cm_{\dot{\alpha}}$	=	dynamic stability coefficients
I_{YY}, I_{XX}, I_X	=	moment inertial, kg $\cdot$ m^2
k	=	surface roughness height, mil
M	=	Mach number
m	=	vehicle mass, kg
$\dot{m}$	=	local wall blowing and ablation rates
p	=	vehicle spin rates, rad/s
q_∞	=	freestream dynamic pressure, kg/m^2
Re_θ	=	momentum-thickness Reynolds number
T	=	air temperature, K
u_e	=	boundary-layer edge velocity, m/s
V	=	freestream velocity, m/s
γ	=	flight path angle, deg
ΔR	=	reentry vehicle impact range miss
ΔV	=	velocity jump due to boundary-layer transition perturbations
θ, ϕ, ψ	=	Euler angles
ζ	=	aerodynamic damping coefficient
δ^*	=	boundary-layer displacement thickness, m
ω	=	natural pitching frequency

I. Introduction

THE knowledge of high-speed boundary-layer transition (BLT) is important for missile engineers because aeroheating and viscous shear stress increase sharply after BLT onset (Figs. 1a and 1b). Unexpected early BLT would increase the heat-shield ablation and the thermal protection weight. One major concern in the entry vehicle design is the variability in the onset of BLT. For instance, the uncertainty in BLT occurrence would result in the vehicle drag coefficient variability and it would in turn cause impact-point dispersion (Fig. 1c). The BLT front can propagate in a manner during reentry, and the resulting ablated shapes exhibit an undesirable configuration (e.g., Fig. 1d). In some cases, the lateral aerodynamic loads would be enhanced due to asymmetric BLT propagation, and the resulting BLT-induced dynamic motions may cause a large entry vehicle impact miss. Another aspect of the BLT phenomenon that affects vehicle design is that of the entry vehicle's radar cross section (e.g., wake observable). The optical signature would be dramatically altered by the advent of BLT. At the present time, we are far from having a good understanding of the mechanisms that could induce the BLT onset, even though it has been extensively investigated over the years in the academic, as well as the defense, industry [1–5]. During the past 40 years, emphasis was placed on flight measurements and wind-tunnel tests to understand the BLT phenomenon. The ground test results were largely used qualitatively, and we found out that care must be taken to extrapolate the ground test results quantitatively to flight environments. Over the years, simple engineering correlations were used by missile engineers to predict the onset of the BLT phenomenon. Table 1 depicts some representative engineering correlations [2,6,7]. Fortunately, over the last decade, significant progress has been made on understanding BLT from its first principles [8]. The linear stability theory (or e^N theory), parabolic stability equation [9–11], and crossflow instability theory have made big strides. Now it has progressed to the degree that commercial aircraft engineers have used them routinely in their designs of wings (e.g., Boeing 777). However, progress has not been extended to high-speed flows, particularly for a vehicle with surface roughness and wall ablation. Based on the published results in the open literature, the mechanism that causes the observed angle-of-attack divergence and trajectory bending has not been clearly established for hypersonic vehicles. For instance, Chrusciel [12] suggested that a relatively small but highly transient body-fixed moment source is the mechanism for the angle-of-attack divergence during boundary-layer transition altitude, whereas Kirsch [13] attributed it to aerodynamic instability (e.g., $Cm_q + Cm_{\dot{\alpha}} \gg 0$). Martellucci and Neff [14,15] singled out the advent of the pitching moment anomalies in the plane of the wind vector as the cause of angle-of-attack anomalies. So far, little analysis has been devoted to connect the impact miss resulting from the BLT perturbation (i.e., angle-of-attack divergence). It will be shown in this paper that a relatively large angle-of-attack divergence during BLT does not necessarily lead to large trajectory bending.

In this paper, focus is on the influence of the BLT phenomenon upon the vehicle flight performance, in terms of its aerodynamics and flight dynamic motions. These include the vehicle's angle-of-attack

Presented as Paper 0309 at the AIAA 45th Aerospace Conference, Reno, NV; received 26 January 2007; revision received 2 July 2007; accepted for publication 28 September 2007.

*Technical Fellow, Mission System/Missile Engineer Center.

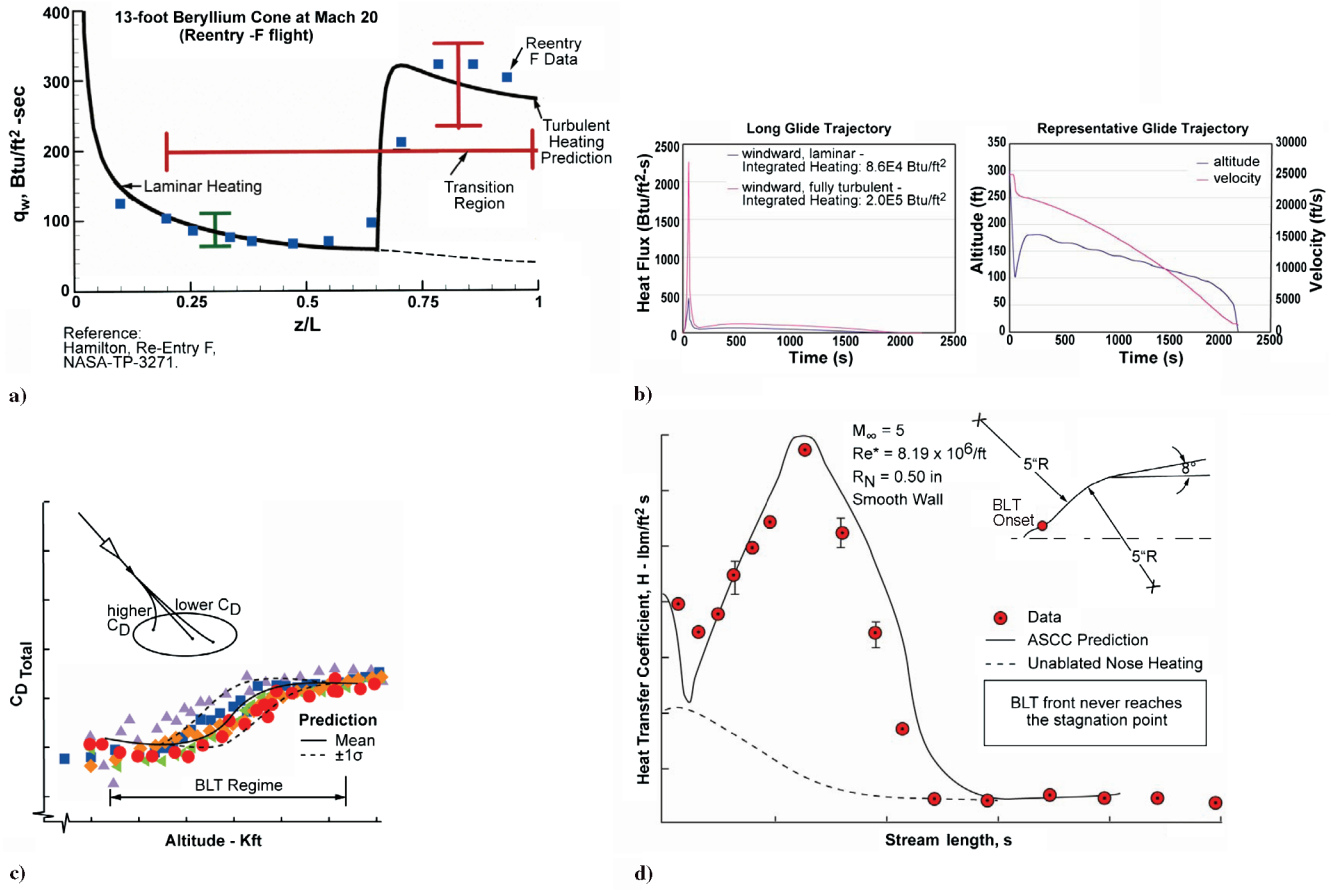

Fig. 1 Some representative examples of the advent of BLT on entry vehicle performances: a) aeroheating rises during BLT, b) uncertainty in predicting the onset of BLT could have a penalty on vehicle TPS weight, c) nonrepeatability of BLT occurrence, and d) BLT effects on nosetip shape evolution.

divergence, the entry vehicle's heat-transfer amplification, and the vehicle's ultimate impact miss. Brief discussion is made on entry vehicle vibrational loads induced by the BLT propagation along the body surface and the associated random pressure fluctuations. This phenomenon would affect the vehicle internal components (e.g., electronics sensors, inertial measurement units, etc.) and aeroshell structural integrity. One objective of this paper is to single out the design approach that would alleviate the adverse effects of BLT occurrence. Some of the potential causes of the BLT onset and its propagation on the entry vehicle are postulated and delineated, and several design strategies to lessen the adverse effects of BLT occurrence are proposed. In Sec. II, assessment is made on the frustum BLT occurrence and its resulting trajectory bending and impact miss. The worst scenario of inducing large ballistic vehicle impact miss is identified. Section III addresses the nosetip BLT phenomenon and its influence on the vehicle performance. The approaches that can be used to lessen the adverse effects of the BLT phenomenon are briefly discussed.

II. Vehicle Frustum Boundary-Layer Transition

A. Vehicle Aerodynamics and Impact Dispersion

When an entry vehicle with smooth surface contours enters deep into the atmosphere, the local air density increases and the laminar boundary finally becomes unstable [2,3,5,6]. The boundary layer evolves into the so-called transitional flow from laminar to turbulent flow and eventually becomes a fully turbulent boundary layer. This process starts at the vehicle base region, and the BLT front propagates from the rear of the entry vehicle toward the nose region. This scenario is referred to as smooth-wall BLT (or wind-fixed or space-fixed disturbance), compared with the BLT induced by surface roughness or "body-fixed disturbance" (see Fig. 2). Based on

Table 1 Estimation of laminar boundary-layer transition onset

Phenomenon	Mechanism	Approach	Correlation
Smooth wall	**Tollmien–Schlichting (mode 1) low Mach**	Engineering correlation (low-recession nosetip correlation)	$\boldsymbol{Re_\theta = C'Me + C''}$
	Tollmien–Schlichting (mode 2) high Mach	Engineering correlation	$\boldsymbol{Re_\theta = C'Me + C''}$
	Tollmien–Schlichting	PST/linear stability	$\boldsymbol{N = 10 \pm 3}$
Entropy and shock-layer vorticity	**Kelvin–Helmholtz instability**	Semi- engineering analysis	$\partial^2 u/\partial y^2 \approx 0$
Roughness-dominated	Surface disturbance and vortex productions	Engineering correlation	$\boldsymbol{Re_K = 250}$
		Engineering correlation	$Re_\theta = 500[(k/\theta)(T_S/T_w)]^{-1.5}$
Crossflow-dominated	Flow profiles with inflection	Engineering correlation	$\boldsymbol{Re_W = 250 \pm 100}$
Wall blowing	Surface disturbance and laminar boundary-layer growth	Engineering correlation	$Re_\theta = 200(1 - 0.05B')\ M_e < 1$ (Apollo data)
Wall blowing and surface roughness	Disturbances from two sources	Engineering correlation	

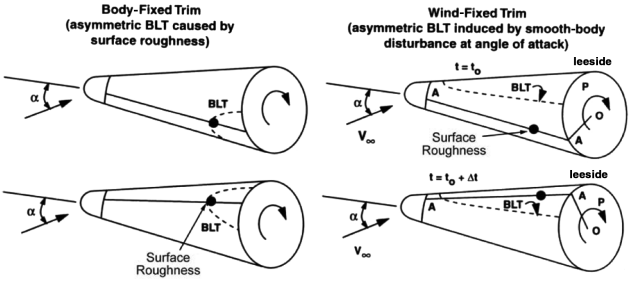

Fig. 2 Trim angles of attack induced by asymmetric boundary-layer transition.

wind-tunnel test results, when an entry vehicle is at the angle of attack, the smooth-wall frustum BLT front is skewed leeside-forward when the vehicle bluntness is slender (bluntness ratio $R_N/R_B < 15\%$). Stetson [16], Holden et al. [17,18], and many researchers' wind-tunnel data† (Fig. 3) confirmed this type of leeward-forward BLT-front distribution. In some blunt-nose cases (e.g., $R_N/R_B < 25\%$), the asymmetric BLT front would actually be skewed toward the windward plane [15,17,18] (see Figs. 4a and 4b). The shift in BLT front from leeward to windward plane was noted by Martellucci [19] and summarized by Schneider [3].

This asymmetric BLT pattern on slender vehicles is found to be valid even at a very small angle of attack (e.g., $\alpha \sim 0.1$ deg). Linear boundary-layer stability theory also predicts this asymmetric BLT pattern (i.e., skewed leeward-forward). When the boundary layer becomes turbulent, the heating rates increase and it results in an increased heat-shield outgassing and ablation for a peripheral segment of the ablative heat shield. This heat-shield ablation would induce nonlinear viscous displacement effects that in turn cause a perturbation in local pressure (see Fig. 5a), and it would affect the static aerodynamic stability [20]. Additionally, Stetson [16] and Schneider [2–4] found that nosetip roughness can affect the downstream frustum BLT onset and propagation (Fig. 5b).

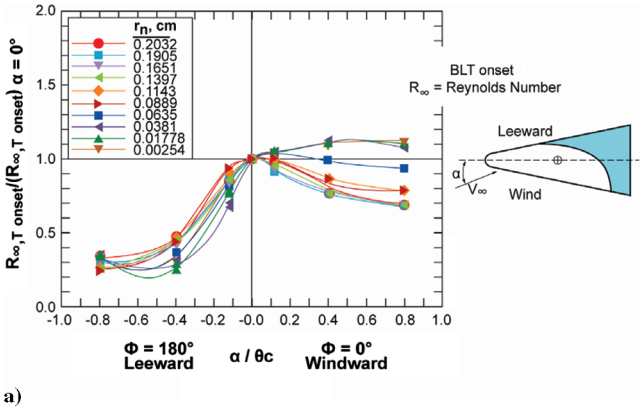

a)

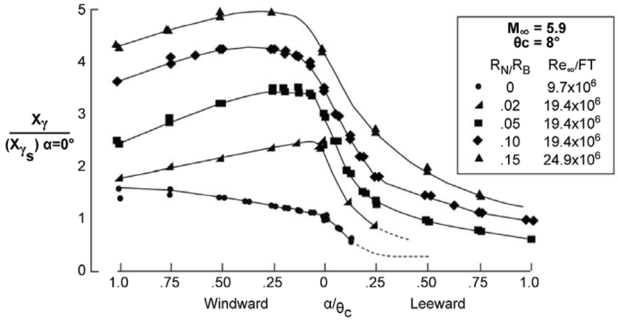

b)

Fig. 3 Transition-front movement with angle of attack: a) according to [17] and b) according to [16].

†Private communication with F.-J. Chen, July 1993.

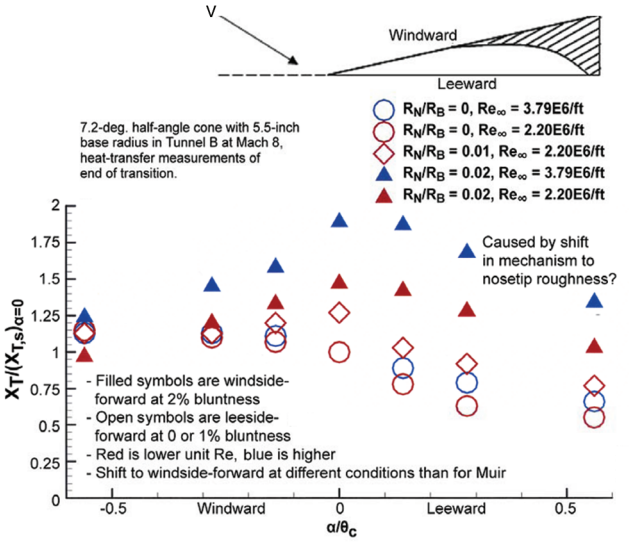

a)

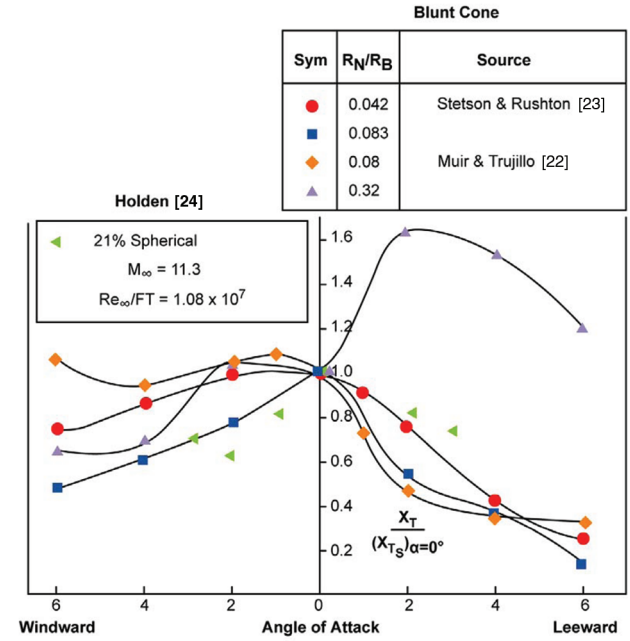

b)

Fig. 4 BLT-front distributions on slender conic bodies at angle of attack: a) transition of blunt cones at angle of attack; shift from leeside-forward to windside-forward (X_T is the surface distance to the transition location) [3] and b) variation of nondimensional transition-front location on blunt cones with angle of attack.

Martellucci [15] found that an unstable pitching moment was measured on an ablated slender cone and the BLT front was skewed leeward-forward. In other words, the static margin of the entry vehicle is reduced (i.e., the center of pressure moves forward during the BLT flight regime). Additionally, when the BLT front is skewed toward the leeward plane forward, transient trim forces and moments are also created by the viscous displacement phenomenon, resulting in an angle-of-attack divergence. This is referred to as BLT angle-of-attack divergence. On the other hand, if the asymmetric BLT front is skewed toward the windward plane forward, the entry vehicle's angle of attack would actually decrease, and the static margin is not affected. Evidently, the latter is the preferred dynamic motion (angle-of-attack convergence), and it was found to occur on a relatively blunt-nose vehicle [as some wind-tunnel data indicated (e.g., Fig. 4b)].

Most entry vehicles are made up of several different segments. At the junction of two segments, a forward- or aft-facing step can exist.

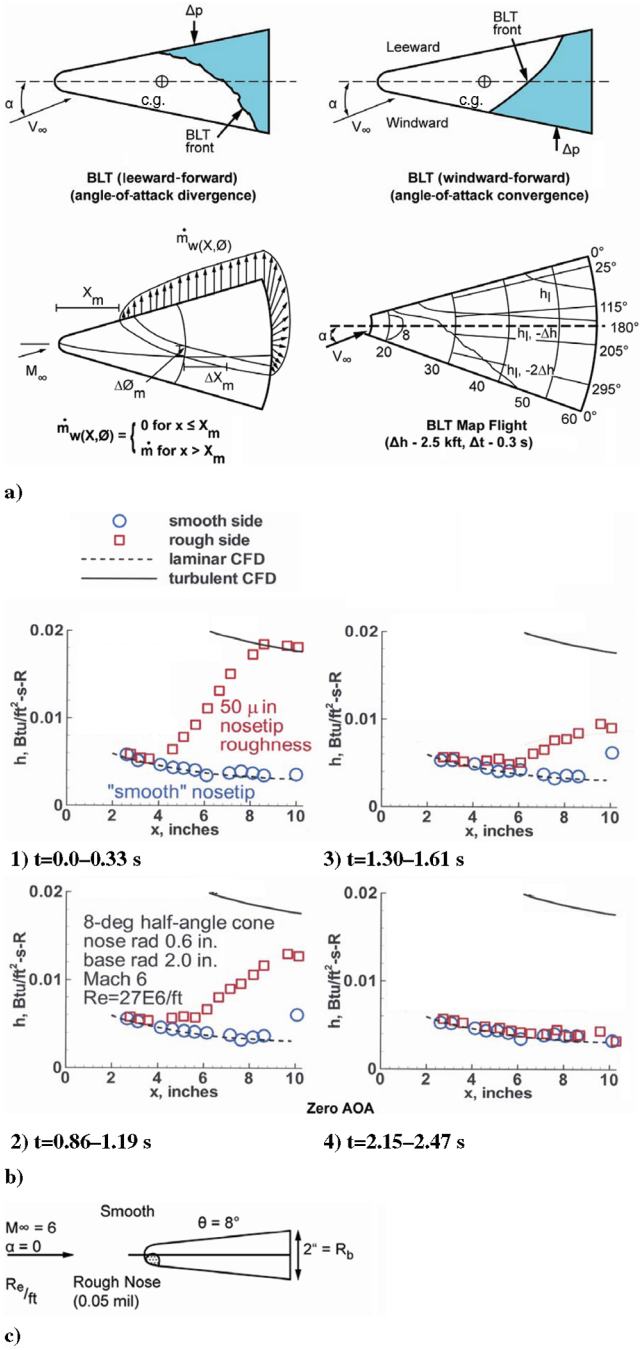

Fig. 5 The influence of surface ablations and surface roughness upon BLT phenomenon: a) frustum boundary-layer transition front propagation, b) nose roughness effect on frustum transition, and c) the higher roughness on one side of the nosetip in plot 1 of Fig. 5b causes frustum transition on the rough side; as the nosetip heats up, the boundary layer thickens and flow returns to laminar (see plot 4 of Fig. 5b).

Additionally, there may be several antenna windows on each vehicle that are made of different materials than the heat-shield frustum material and they will ablate at different rates than the frustum heat-shield materials. At times, the different thermal expansion between the two nonhomogeneous thermal protection system (TPS) materials would induce a surface contour distortion. These types of surface irregularities (sometimes referred to as banana effects) can act as a boundary-layer trips, causing the BLT phenomenon to occur at a higher altitude than with a smooth heat-shield surface. Usually, a good vehicle design would keep these types of surface irregularities to a minimum. These types of surface irregularities are referred to as body-fixed disturbances.

So far, we have identified the trim forces and moments, which can be body-fixed (e.g., the antenna windows or the backward-facing steps) or wind-fixed (e.g., smooth-wall BLT front skewed leeside-forward). It is important to recognize that the transient angle-of-attack divergence only results from an asymmetric BLT front that has a skewed leeward BLT front. So to avoid the angle-of-attack divergence, a vehicle with an asymmetric BLT front skewed windward-plane-forward is preferred. Currently, some evidence indicates that the nosetip bluntness ratio or nosetip roughness effects may play a role in the occurrence of the windward-forward BLT front. More wind-tunnel tests are needed to confirm this observation.

To eliminate this flow asymmetry, boundary-layer trips are proposed to trip the laminar boundary evenly, or symmetrically [8]. Several wind-tunnel tests were conducted to validate the trip concept. Preliminary results are encouraging. The downside of the BLT trips approach is that it increases the vehicle drag forces and the total integrating heating, and therefore it increases the TPS weight.

Next, possible mechanisms during the BLT altitude that induce large trajectory bending (deflections) or large transverse velocity ΔV are discussed. The trajectory bending for a ballistic entry vehicle is defined as [24,25]

$$\Delta\gamma = \frac{\Delta V}{V_\infty} \tag{1}$$

and the impact miss due to BLT perturbation, ΔR, is defined as

$$\frac{\Delta V}{V_\infty}\frac{h}{\sin^2\gamma} \tag{2}$$

A small value in ΔV can cause a significant impact miss. For instance, at the 80-kft altitude, with $\Delta V = 15$ ft/s, $V = 18,000$ ft/s, on a flight path angle of $\gamma = -25$ deg, the downrange miss can be of the magnitude of

$$\Delta R \sim \frac{\Delta V}{V_\infty}\frac{80,000}{(\sin\gamma)^2} \sim 380 \text{ ft}$$

For a spin-stabilized vehicle during entry, the lifting forces are averaged out through the vehicle's precession motion. Figure 6

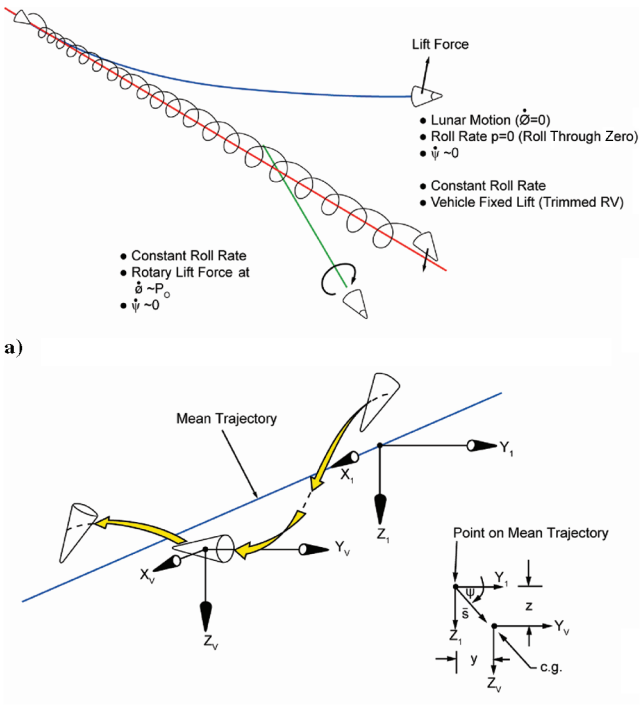

Fig. 6 Spinning ballistic entry vehicle flight dynamics: a) schematic of a ballistic reentry vehicle (RV) with helix motion (precession/coning motion) and b) motion of the c.g. about the mean flight path.

depicts a vehicle in precession/nutation angular motion. The entry vehicle's transverse velocity perpendicular to the flight path can be calculated as

$$\Delta\bar{V} = (\Delta v)\bar{i} + (\Delta w)\bar{j} = -\frac{1}{m}\int_{t1}^{t2} C_L q_\infty A e^{i\psi}\,\mathrm{d}t \tag{3}$$

where $\Delta\bar{V}$ is the transverse velocity, m is the entry vehicle mass, C_L is the lift-force coefficient, ψ is the precession angle, $\int \dot{\psi}\,\mathrm{d}t$ is the Euler angle, $\dot{\psi}$ is the precession rate, A is the entry vehicle base area, and q_∞ is the freestream dynamic pressure. A large ΔV can result from lift-force nonaveraging, such as when ψ is a constant (i.e., $\dot{\psi} \sim 0$) or there is a step change in the lift force. From the classical Euler angle relation, the precession rate $\dot{\psi}$ can be related to the spin rate and windward meridian rotation rates; that is,

$$\dot{\psi} = p - \dot{\phi} \tag{4}$$

where p is the entry vehicle spin rate, and $\dot{\phi}$ is the rate of the windward meridian change. Therefore, when an entry vehicle is in trimmed motion or lunar motion ($\dot{\phi} \approx 0$), the precession $\dot{\psi} \approx p$, then a lift-vector-averaging process would occur. Consequently, the ΔV will not be a large value and it results in a small trajectory bending. On the other hand, when $\dot{\psi} \to 0$ (or ψ is constant), there is no lift-vector averaging, and a larger trajectory bending would occur. In this event, it requires $p \approx \dot{\phi}$, or else windward meridian is rotary and is opposite of the spin rates. A closed-form solution can be found to estimate the aerodynamic jump for the special case of trim windward meridian (the so-called lunar motions $\dot{\phi} = 0$ and $p = \dot{\psi}$) during the BLT regime, which yields [24,26]

$$\Delta V = \frac{C_L q_\infty A}{mp}\left(1 - \frac{p^2}{p_{\mathrm{crit}}^2}\right)\frac{\sin(p\Delta t/2)}{p\Delta t/2} \tag{5}$$

where Δt is the flight interval in which the asymmetric BLT event exists, and p_{crit} is the entry vehicle's natural pitch frequency:

$$\left[\frac{Cm_\alpha q_\infty AD}{I_{YY} - I_{XX}}\right]^{1/2}$$

For a ballistic entry vehicle, the lift vector is rotating at a precession rate of $\dot{\psi}$. Then the parameter of spin rate p in Eq. (5) should be replaced by $\dot{\psi}$ instead. Table 2 lists some representative aerodynamic jumps (ΔV values) for different magnitudes of Δt, entry vehicle mass m, spin rate, and freestream dynamic pressure during the BLT flight regime. The table shows that the aerodynamic jump ΔV is larger at lower spin rates, with higher freestream dynamic pressure, and at small BLT-perturbation times. A larger Δt implies a longer BLT propagation time along the vehicle frustum. These results show that higher spin rates and heavier entry vehicles experience lower induced ΔV, resulting in smaller angles of attack and smaller trajectory bending.

A 6-DOF flight simulation was made for a representative blunt entry vehicle, with a ballistic coefficient $\sim$2000 lb/ft^2 and a set of Newtonian aerodynamics. The first case considered is that the entry vehicle is in lunar and trim motions during the BLT regime. Figure 7 depicts the 6-DOF numerical results. The trim angle of attack is assumed to be $\alpha_{\mathrm{trim}} \sim 1.0$ deg, and the lift coefficient is assumed to be $C_L = 0.035$ (a Newtonian value). Figure 7a depicts the windward meridian history, and it shows the windward meridian rate $\dot{\phi} \sim 0$ during the the BLT altitude. Figure 7b shows the angle-of-attack divergence during the BLT flight regime, and the angle of attack reaches a little above the trim angle of $\alpha_{\mathrm{trim}} \sim 1.0$ deg. The vehicle experiences a peak lateral load of $\sim$9 g (Fig. 7c). The corresponding transverse velocity perturbations are $\sim$8 m/s (see Fig. 7d).

In some special cases, shown in Fig. 8a, the entry vehicle is not in lunar motion (i.e., windward meridian, $\dot{\phi} \neq 0$), as illustrated in Fig. 7. Instead, the vehicle exhibits a rotary motion during the BLT regime instead (Fig. 8a). This resulting vehicle dynamic behavior is different from the case shown in Fig. 7. Figure 8b shows that the maximum angle of attack is about the same: $\sim$1.0 deg at the 22-km altitude. The maximum lateral acceleration is about 8 g at the BLT altitude. However, the transverse velocity has a relatively large jump ($\Delta V \sim 70$ m/s) at the 22-km altitude, where a wind-fixed disturbance was imposed (Fig. 8a). This case illustrates that a wind-fixed perturbation with an asymmetric BLT front skewed *leeward* forward can induce a large entry vehicle trajectory deflection, even for small angle-of-attack divergence.

Simple analytical solutions were derived to validate the numerical 6-DOF results. The classical Euler equations (θ, ψ, ϕ) for a rigid body can be written as [25,26]

$$\begin{aligned} I\frac{\mathrm{d}^2\theta}{\mathrm{d}t^2} + I_X p\dot{\psi}\sin\theta - I\dot{\psi}^2\sin\theta\cos\theta + 2I\zeta\omega\dot{\theta} &= Cmq_\infty AD \\ &\quad + Cm_{\mathrm{body}}\cos\phi q_\infty AD \\ I\frac{\mathrm{d}(\dot{\psi}\sin^2\theta)}{\mathrm{d}t} - I_X p\sin\theta\dot{\theta} + 2I\zeta\omega\dot{\psi}\theta^2 &= Cnq_\infty AD \\ &\quad + Cm_{\mathrm{body}}\sin\phi q_\infty AD \end{aligned} \tag{6}$$

where ζ is the entry vehicle aerodynamic damping, Cn is the out-of-plane moment, and Cm is the in-plane pitching moment $(Cm_\alpha\alpha + Cm_{\mathrm{wind}})$.

The Euler coordinate is depicted in Fig. 9. During the BLT altitude, when $Cm_{\mathrm{body}} = Cn = 0$, θ is small ($\theta \ll 1$) and $I_X/I \ll 1$, then Eq. (7) can be simplified to

$$\frac{\mathrm{d}}{\mathrm{d}t}(\dot{\psi}\theta^2) = -2\zeta\omega\dot{\psi}\theta^2 \tag{7}$$

or it can be integrated as

$$\dot{\psi} = \dot{\psi}_0\left(\frac{\theta_0}{\theta}\right)^2 \exp(-2\zeta\omega t) \tag{8}$$

Therefore, with no body-fixed trim moment, the precession motion $\dot{\psi}$ is quickly damped to zero exponentially in a high-dynamic-pressure environment. Also, if the angle of attack θ is increased rapidly due to BLT wind-fixed perturbation, such as a smooth-wall asymmetric transition front, the precession rate will be decreased as $(\theta_0/\theta)^2 \to 0$ when the wind-fixed trim θ is much bigger than the initial angle of attack θ_0. This simple closed-form solution explains the large ΔV found on the case in which wind-fixed disturbance is dominant over the body-fixed trim forces.

The second candidate mechanism for inducing large ΔV is a rapid change in lift force, such that the precession motion would not

Table 2 Trajectory bending as functions of spin rates, disturbance time, and vehicle mass

Case	p, deg/s	Δt, s	q_∞, lbf	A, ft^2	m, lb	C_L	p_{crit}, Hz	ΔV, fps
1	360	0.3	50,000	2	300	0.035	5	73.9
2	360	0.3	30,000	2	600	0.035	5	44.3
3	360	0.15	30,000	2	600	0.035	5	49.8
4	360	0.075	30,000	2	600	0.035	5	51
5	180	0.3	30,000	2	600	0.035	5	102.6
6	720	0.3	30,000	2	600	0.035	5	11.4
7	100	0.3	30,000	2	600	0.035	5	204.7
8	10	0.3	30,000	2	600	0.035	5	1850.5

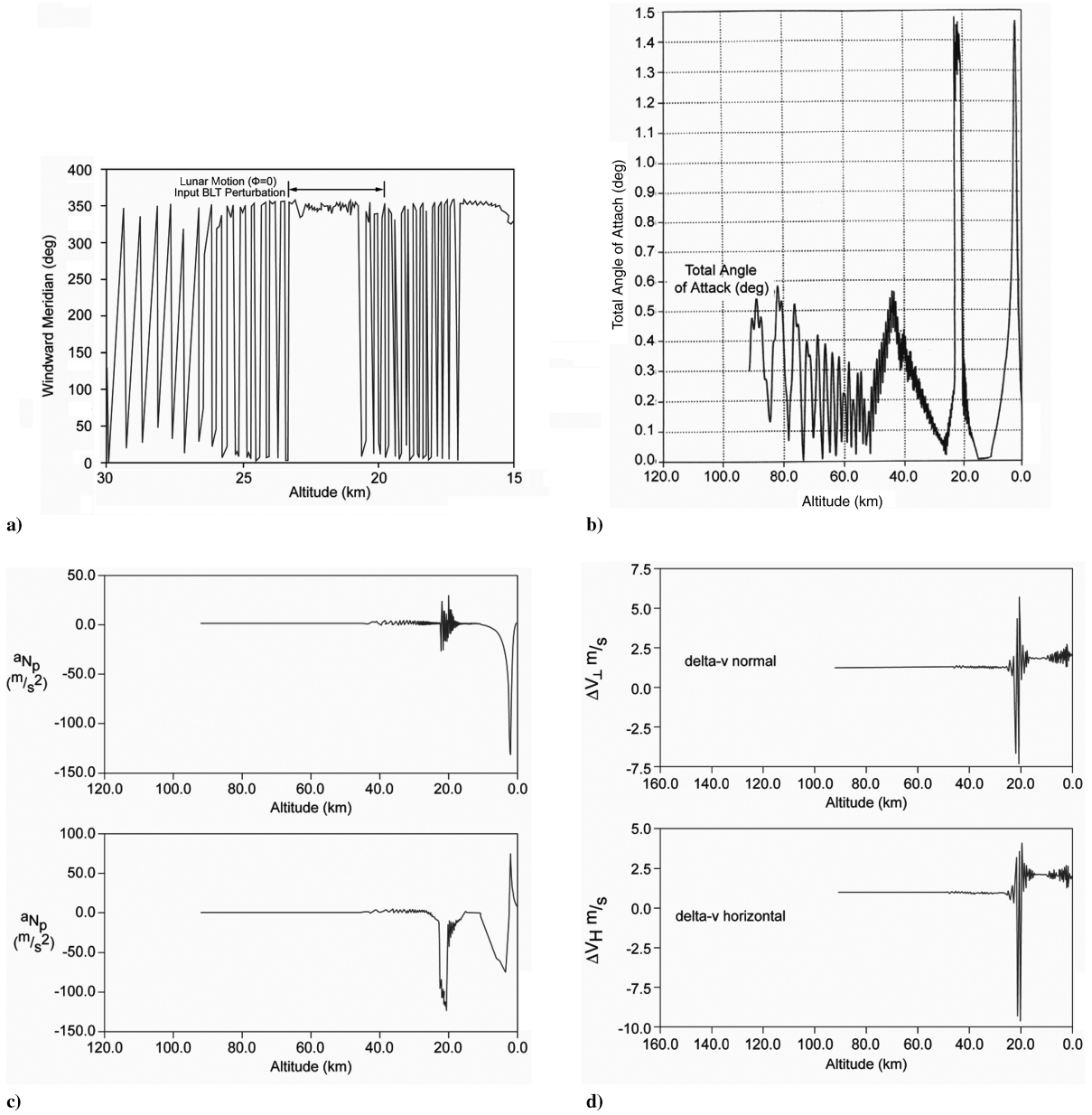

Fig. 7 Entry vehicle flight dynamics with body-fixed disturbances: a) windward meridian history for the RV with body-fixed disturbance (lunar motion) during the BLT altitude, b) angle-of-attack history for the RV with wind- and body-fixed disturbances during the BLT altitude, c) lateral acceleration history for the RV with body-fixed disturbance during the BLT altitude, and d) transverse velocity perturbation during BLT for the RV with body-fixed disturbance.

average out the impulsive motion. During the BLT, the pitching frequency is about 5 to 12 Hz. The time scale for this impulsive motion must be shorter than 0.05 s to cause significant impact miss.

To alleviate the adverse effects of asymmetric BLT-induced impact miss, several approaches can be made. The first one is to select an entry vehicle configuration that would render a windside-forward BLT front. Some wind-tunnel data suggest that the nose bluntness ratio and nosetip roughness play a role in determining whether the BLT front would tilt windside- or leeside-forward. More wind-tunnel tests are needed to ascertain that the asymmetric BLT front is skewed windside-forward. The second approach is to insert boundary-layer trips at the forward part of the frustum (see Fig. 10). This approach has been undertaken in many wind-tunnel testings [27] in which a laminar boundary layer would exist in the natural and unperturbed environment. Properly selected BLT trips are inserted near the nose region. These boundary-layer trips would cause a transition front to propagate quickly from the rear section to the front of the vehicle section without going through the asymmetric BLT-front propagation. The trip heights can be selected from the following simple engineering correlation [27]:

$$\frac{k}{\delta^*} \approx 3 \tag{9}$$

where k is the trip height, and δ^* is the local boundary-layer displacement thickness. It is noted that the boundary-layer displacement thickness is a function of altitude; therefore, one can tailor the desired BLT altitude with a relevant boundary-layer trip height. Evidently, the tripped BLT altitude will be higher than the smooth-wall natural transition altitude. The third approach is to select a trajectory to minimize the BLT effects. This is the so-called trajectory optimization.

B. Frustum BLT-Induced Vibrational Loads

High-performance entry vehicles are subject to an intense fluctuating pressure field during reentry flight, which can affect the integrity of the vehicle structure and impose adverse vibrational loads on internal components. These random pressure fluctuations arise from the instability and unsteady motion of fluid flow within the transitional/turbulent boundary layer. Several hypotheses have been

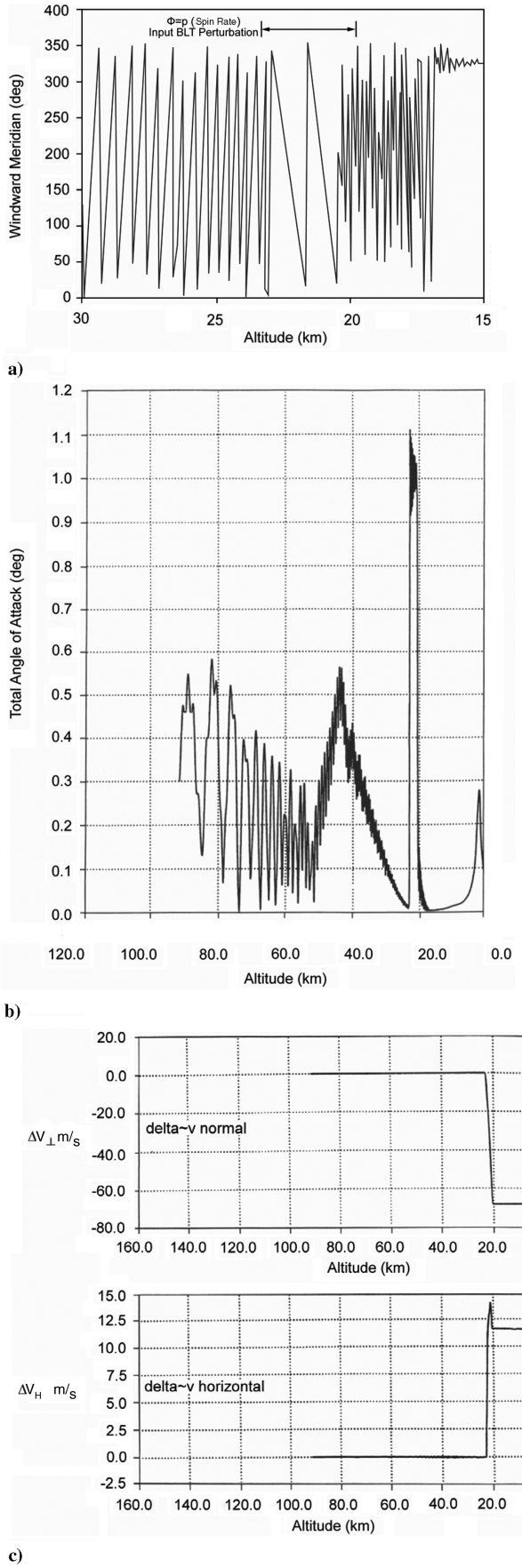

Fig. 8 Entry vehicle flight dynamics with wind-fixed disturbances: a) windward meridian history for the RV with wind-fixed disturbance during the BLT altitude, b) angle-of-attack history for the RV with wind-fixed disturbance during the BLT altitude, and c) transverse velocity perturbation for the RV with wind-fixed disturbance during the BLT altitude.

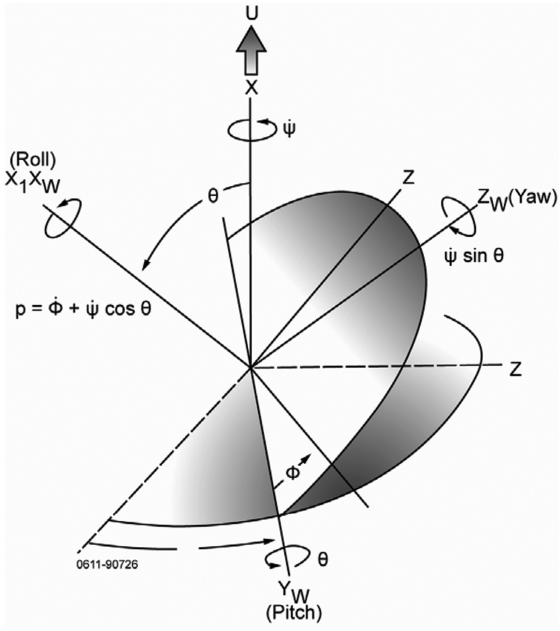

Fig. 9 Euler coordinate.

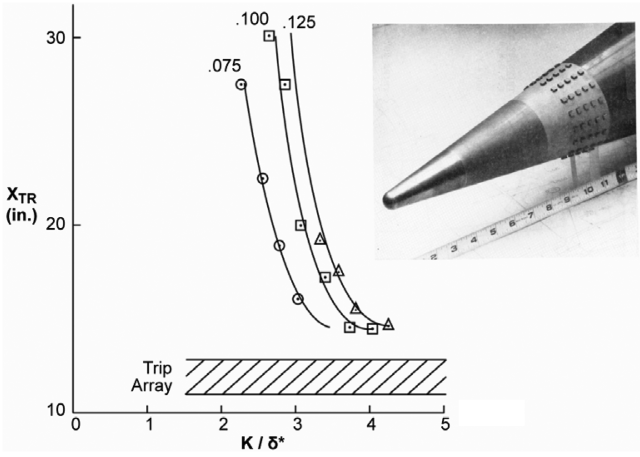

Fig. 10 Design of a boundary-layer trip.

proposed to describe this random motion of the momentum-deficient fluid. Those studies were mostly focused on the intermittent eruptions of the viscous sublayer. This complicated phenomenon is still only vaguely understood, and design criteria have been developed primarily on the basis of experimental data. After knowing the pressure fluctuations, finite element analysis is performed on the vehicle substructure to translate these random perturbations to vehicle vibrational loads.

The acoustic levels on the entry vehicle aeroshell/substructure are very low preceding boundary-layer transition. However, a rapid increase in levels occurs after BLT onset, followed by a localized peak in the level. Based on the wind-tunnel data and past flight data, the acoustic levels during transition are expected to be approximately 10 dB higher than would be expected for fully developed turbulence at the same dynamic pressure, edge velocity, and boundary-layer thickness. The progress of transition from aft to the forward section of the vehicle was detected by the acoustic sensors on many flights. In general, the vibration levels at internal locations (e.g., the instrumentation shelf) are below those on the aeroshell. However, they show comparable trends with high levels occurring at transition altitude. Attention must be paid to the aeroshell structure design, because shell resonance would occur at lower frequency (1 to 10 KHz) during the BLT altitude regime. A significant feature of this aeroshell random vibration resulting from the transitional

boundary-layer pressure fluctuation is the high acceleration levels; fortunately, the predominately energy is located at a relatively high frequency. The power spectrum density level in the range of 0.1 g^2/Hz is common for frequency above 10 KHz. At lower frequency, an acceleration level of this magnitude would be a very severe environment for vehicle internal components such as onboard instruments (e.g., fuze or radar) and electronic devices (e.g., inertial measurement units). The magnitudes of the vibrational loads during the BLT flight regime would depend on the boundary-layer edge dynamic pressure, vehicle configurations, local boundary-layer thickness, and boundary-layer edge Mach number. Currently, the conventional approach in high-speed-flow regimes is to use flight measurements to specify this environment.

To alleviate this high random-vibration environment, attenuation blankets were inserted to surround the internal components and to isolate them from the high-frequency and high-level shell-vibration environments. Finite element analysis and ground tests are needed to certify this design approach. Those attenuation blankets are available in commercial markets.

III. Blunt-Nose Boundary-Layer Transition

A. Nose BLT on Ablated-Nose Performance

The phenomenon of BLT occurrence on a blunt nose in hypersonic and supersonic flows is different from that on the frustum [2–5,28,29]. In the nosetip region, the flows are subsonic, and if the surface is smooth, according to the linear stability theory, the BLT is dominated by the first mode (Tollmien–Schlichting waves). Because the streamlines are curved, Gortler instability can be important. In high-speed flows, the nose BLT is induced by the thermal protection materials' surface roughness and the associated wall blowing. For instance, on the Apollo flight, the nose BLT occurred at the ~210-kft altitude. The boundary-layer transitional flow correlation parameters $Re_\theta/M_e \leq 200$ under no heat-shield ablation conditions, shown in Fig. 11a, suggested that the flow was far from unstable. Bartlett et al. [30] suggested that the heat-shield ablation on the Apollo nosecap may have been triggered by an earlier boundary-layer transition due to the wall blowing. In their calculations, the boundary-layer ablation parameter

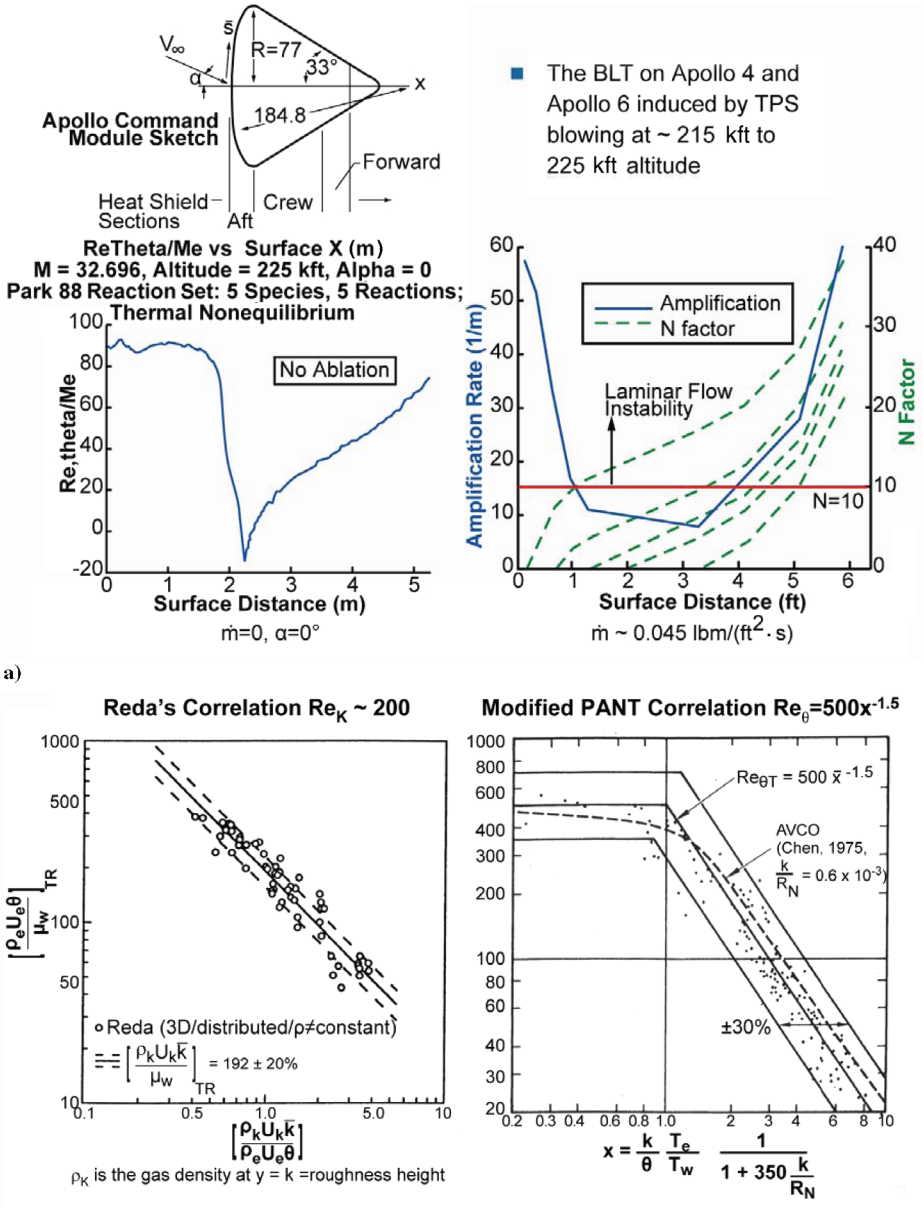

Fig. 11 Nosetip BLT onset correlation, including effects of wall blowing and surface roughness: a) wall blowing effects on boundary-layer transition and b) nosetip transition (3DC/C, graphite); roughness-dominated.

$$B' = \frac{\dot{m}}{\rho_e u_e Ch} = 4 - 6$$

where Ch is the local heat-transfer coefficient, including the wall blowing effects.

Apollo's TPS material was AVCOAT-5026. At the 210-kft altitude, heat-shield surface sublimation was nil, yet AVCOAT-5026 had in-depth charring and pyrolysis. The resulting B' reached 4 or higher [30]. It is speculated that Apollo's wall might not be smooth at the BLT altitude because of the in-depth charring and pyrolysis phenomenon that can roughen the wall. The advent of surface roughness might partially be responsible for the BLT onset on Apollo flight. Further studies are needed on this subject.

Reda [5] conducted ballistic-range tests and concluded that the surface roughnesses on the graphite and 3D carbon–carbon nosetips play important roles in the development of BLT onset. He suggested a roughness Reynolds number criterion for BLT onset in the nosecap region (i.e., $Re_K = 250$, where k is the wall roughness height (see Fig. 11b).

Some other nose BLT onset criteria were developed over the years and they were used successfully in predicting the nosetip BLT onset (Fig. 11b). They can be correlated as

$$Re_\theta = C'\left(\frac{k}{\theta}\frac{T_e}{T_w}\right)^{-m} \tag{10}$$

where C' and m are empirical constants that have to be determined from ground-test results, T_e is the boundary-layer edge temperature, and T_W is the wall temperature. From the wind-tunnel tests, arc tests, and ballistic-range tests, these constants were found to have the following values: $C' = 200$ to 750 and $m = 0.7$ to 1.5. The values of the constant C' and m can affect the predicted nose-ablation history and the nose-region BLT altitude. It should be pointed out that Eq. (10), sometimes referred to as the modified passive nosetip program (PANT) BLT correlation, can be derived from Reda's [5] critical roughness Reynolds number criterion (i.e., $Re_K = 250$). Figure 12 depicts a 2-in. spherical nosetip shape-change history during a high-speed reentry. The nosetip laminar boundary-layer wall roughness was assumed to be $k = 0.25$ mil in this example. When $C' = 700$ and $m = 1.35$, the nosetip remains laminar during entry flight until at impact. The total stagnation-point ablation is ~0.29 in. Its ablated shape is classified as a laminar blunt configuration (Fig. 12a). With $C' = 371$ and $m = 1.0$, the nosetip exhibits the so-called indented shape (see Fig. 12b). In this case, the boundary-layer transition has occurred near the sonic point, the stagnation point remains in laminar flow, and the stagnation-point ablation is still ~0.29 in. Finally, with $C' = 215$ and $m = 0.7$, the nosetip is predicted to be fully turbulent below the 15-kft altitude (Fig. 12c). The nose shape has evolved into the turbulent equilibrium shape. The nose stagnation-point ablation reaches ~0.80 in. In this example, it demonstrates that the magnitude of nose ablation and its ablated shapes are determined by the nose transition altitude and its

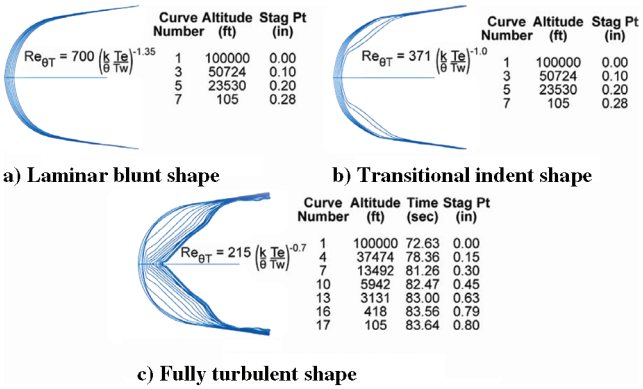

Fig. 12 Dependence of shape-change prediction during reentry on the correlation model; $R = 2.0$ in. and $k = 0.25$ mil.

BLT-front propagation. The resulting drag coefficients would be influenced by the nose ablation as well. Therefore, nosetip transition onset and its front propagation play important roles in the low-altitude ablated-nose performance. The selection of thermal protection material is vital to entry vehicle design.

The potentially different ablated-nose shapes are depicted in Fig. 13. These nose shapes are the outcome of various BLT-front propagations on the nose region. They can be classified as the laminar blunt shape, mildly indented shape, severely indented shape, unsteady flow shape, and the eventual turbulent equilibrium shape. The unsteady flow shape was tested in the Calspan Corporation's shock tunnel and the flows were found to be pulsating with a Strouhal number of ~0.25. These sinusoidal vibrational loads can be severe enough to affect the entry vehicle's internal payload structural integrity. For a nose of radius ~1 in., this vibrational phenomenon would occur at frequencies exceeding 10 KHz. Vehicle designers must take this factor into consideration. The other salient features of this ablated shape are the appearance of imbedded shocks and a locally separated boundary layer in the indented region. Under certain circumstances, the complex flow pattern of Edney's jet may appear. The consequence of these complicated flow patterns is the increase of local heating by a factor of 10 and higher, which would affect the vehicle's aerodynamic stability, as will be discussed later.

B. Nose BLT on Aerodynamic Stability

Another important influence of this ablated shape is its strong effects on an entry vehicle's aerodynamic stability. Figure 14 shows the wind-tunnel data on a blunt conic body's center-of-pressure location with various ablated-nose shapes. The test model is a blunt 6-deg cone with a bluntness ratio of 20 to 25%. The test conditions are a freestream Mach number of 11.8 and unit Reynolds number of $Re/\text{ft} = 10.7 \times 10^6$. The test results indicated that a change of center-of-pressure location can be ~5 to 7% on a severely indented nose or on an unsteady nose shape. This large reduction in the static aerodynamic stability due to the nose ablation resulting from nose BLT is of great concern for entry vehicle designers. Therefore, these types of indented shapes should be avoided in a good entry vehicle design.

C. Asymmetric Nose BLT

In addition to the effects on the aerodynamic stability, the nose ablation does not occur in an axisymmetric fashion, it usually evolves in an asymmetric way. One example is the nosetip-recovered vehicle (NRV) nose shown in Fig. 15, which went through an intermediate-range ballistic missile flight trajectory and was "softly" recovered below the 20-kft altitude. The figure shows that the ablated-nosetip shapes were not symmetric in the four quadrants (i.e., $\phi = 0$-, 90-, 180-, and 270-deg azimuthal planes). This asymmetry would cause the creation of a trim angle of attack, which in turn results in unwanted lateral aerodynamic loads. Therefore, in the entry vehicle design, it is desirable to control the nose BLT onset altitude (as well as the BLT-front propagation) and its ablated pattern symmetry. The selection of the nosetip TPS material and its size are crucial to the control of BLT and its effects on vehicle performance.

Over the years, several approaches were devised to make nosetip BLT phenomenon become more predictable and the ablated-nose shape more symmetric. The design approaches were called shape-stable nose (SSN) designs. One approach is to place many small depressions or small cavities (or small craters) on the surface of the nose. Figure 16 depicts this "holey-nose" configuration. This idea was motivated by the observation that a small cavity in the nose subsonic region would act as a boundary-layer trip. Placing distributed holes in the subsonic region would trip the nosetip laminar boundary layer evenly to turbulent flows. This would avoid the development of an asymmetric nose BLT event. Extensive arc tests indicated that this approach is feasible. A second proposed approach is to place rough surface material between the stagnation region and the sonic point, such that the wall roughness would trip the laminar boundary layer earlier and evenly in the nose region during entry flight. These two SSN designs were proposed in the entry

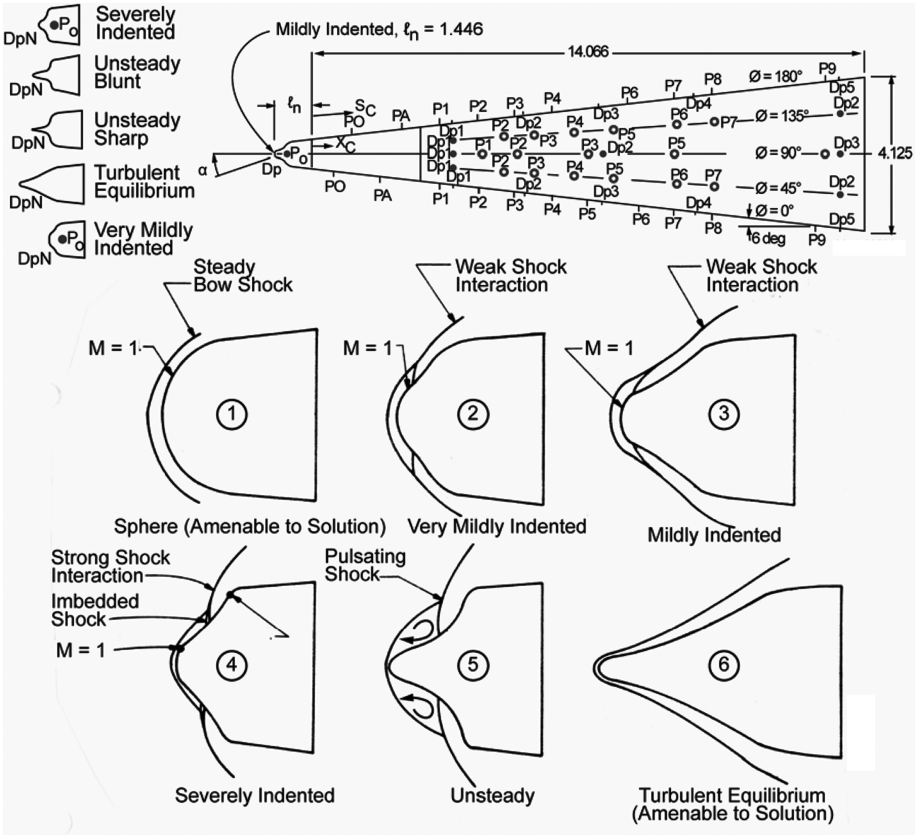

Fig. 13 Schematic drawing of nosetip configurations resulting from different nose BLT propagations.

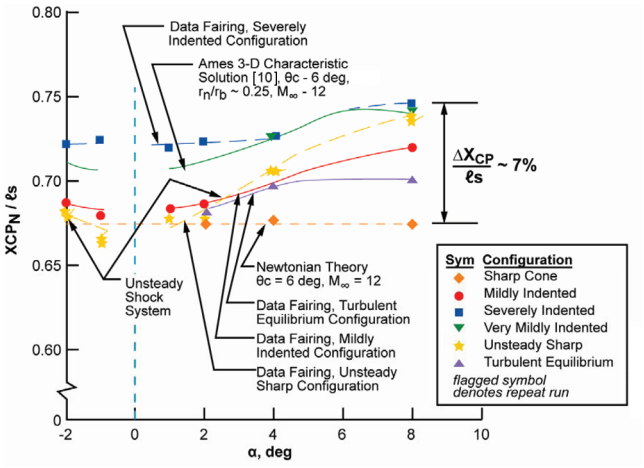

Fig. 14 Nose and angle-of-attack effects on center of pressure; $M_\infty \approx 11.8$ and $Re_\infty/\text{ft} \approx 10.7 \times 10^6$.

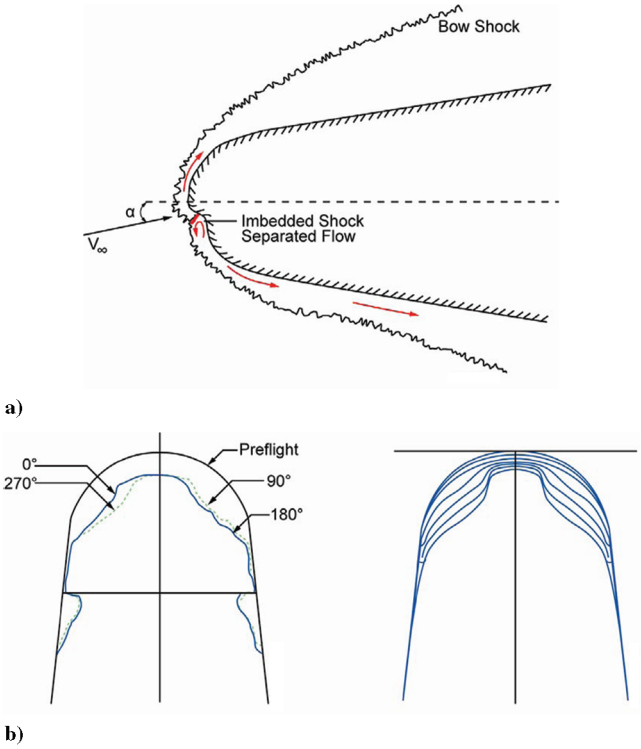

Fig. 15 Asymmetric nose ablation on entry vehicles: a) schematic showing a predicted asymmetrically ablated nose shape and b) NRV nose shape.

vehicle designs and ground tests indicated that they are viable concepts. Flight simulations also render smaller trim angles of attack and lower roll trim loads during nose BLT events.

IV. Conclusions

A review of influence of the boundary-layer transition phenomenon upon a high-speed entry vehicle performance is made. In addition to the heating augmentation and viscous drag increases associated with the advent of turbulent boundary layer, focus is on other aspects of vehicle performance: flight dynamics, aerostability, lateral trim loads, and impact dispersion. The major technical concerns with BLT phenomenon are 1) the uncertainties in the BLT onset, 2) the prediction of the BLT-front propagation along the body vs altitude, 3) the advent of an asymmetric BLT front from the windward to leeward planes, and 4) the repeatability of the BLT events. In general, it appears that surface roughness and wall blowing play an important role in the onset of laminar boundary-layer transition on the frustum and on the nose region. It is noted that on the

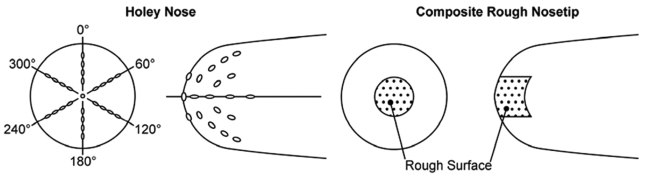

Fig. 16 Shape-stable nosetip design.

frustum BLT, a windward-forward BLT front is preferred, to cause a decrease in aerodynamic stability and to prevent angle-of-attack divergence. Also, a body-fixed BLT perturbation is better than a wind-fixed BLT front. At the present time, it is not clear how to achieve a windward-forward BLT front on the frustum. Most of the wind-tunnel data suggested a leeward BLT-front distribution on a slender body. Some wind-tunnel results indicated that nose bluntness plays a role. It seems that a very blunt vehicle ($R_N/R_B > 15\%$) has a tendency to exhibit a windward-forward BLT front. Stetson [16] observed that the nosetip roughness heights and distributions can be important for the downstream frustum BLT onset. To alleviate the adverse effects of frustum BLT, careful selection of entry vehicle configuration is important (particularly, the bluntness ratio). The application of boundary-layer trips on the forward frustum can be made to ascertain that the BLT event is predictable and repeatable and that the BLT front is symmetric. For nosetip boundary-layer transition onset and propagation, the TPS material laminar surface roughness and its wall blowing are important.

The modified PANT correlation [Eq. (10)] or the roughness Reynolds number ($Re_K \sim 200$) correlation appears to be adequate for ablating 3D carbon–carbon and graphite nosetip materials. However, it requires knowing the values of roughness height for the TPS material of interest. Usually, that representative roughness height is not known. Ground tests and flight tests are needed. The influence of the nosetip BLT onset and the associated nosetip ablation on the entry vehicle's heating augmentations, aerodynamic stability, and the trim aeroloads are illustrated through wind-tunnel measurements and analytic predictions. It is not desirable to have the nose BLT occurring near the sonic point, staying there, and not propagating to the stagnation point during entry flight. This situation would result in indented nose shapes and the so-called laminar islands. In most instances, an asymmetric shape would result and trim angle of attack would be a cause of concern. The approaches to decrease the adverse effects of nosetip BLT are either by placing distributed surface craters in the nose region (a holey nosetip) or by inserting high-roughness-height material near the stagnation region.

References

[1] Reshotko, Eli, "Boundary Layer Instability, Transition and Control," 32nd Aerospace Sciences Meeting, Reno, NV, AIAA Paper 94-0001, 10–13 Jan. 1994.

[2] Schneider, S. P., "Flight Data for Boundary Layer Transition at Hypersonic and Supersonic Speeds," *Journal of Spacecraft and Rockets*, Vol. 36, No. 1, 1999, pp. 8–20.

[3] Schneider, S. P., "Hypersonic Laminar-Turbulent Transition on Circular Cones and Scramjet Fore Bodies," *Progress in Aerospace Sciences*, Vol. 40, Nos. 1–2, 2004, pp. 1–50. doi:10.1016/j.paerosci.2003.11.001

[4] Schneider, S. P., "Laminar-Turbulent Transition on Reentry Capsule and Planetary Probes," AIAA Paper 2005-4763, June 2005.

[5] Reda, D.C., "Review and Synthesis of Roughness Dominated Transition Correlation for Reentry Applications," *Journal of Spacecraft and Rockets*, Vol. 39, No. 2, 2002, pp. 161–167.

[6] Muramoto, K., "Algebraic Correlation for High-Speed Transition Prediction on Sphere Cones," *Journal of Spacecraft and Rockets*, Vol. 40, No. 4, 2003, pp. 598–600.

[7] King, R. A., "Mach 3.5 Boundary Layer Transition on a Cone at Angle of Attack," 22nd AIAA Fluid Dynamics, Plasma Dynamics and Laser Conference, Honolulu, HI, AIAA Paper 91-1804, June 24, 1991.

[8] Nestler, D. B., and McCauley, W. D., "A Study of a Boundary Layer Trip Concept at Hypersonic Speeds," AIAA Paper 81-1086, June 1981.

[9] Malik, M. R., Spall, R. E., and Chang, C. L., "Effect of Nose Bluntness on Boundary Layer Stability and Transition," 28th Aerospace Sciences Meeting, Reno, NV, AIAA Paper 1990-112, 8–11 Jan. 1990.

[10] Reed Helen, L., and William S. Saric, "Linear Stability Theory Applied to Boundary Layer," *Annual Review of Fluid Mechanics*, Vol. 28, 1996, pp. 389–428. doi:10.1146/annurev.fl.28.010196.002133

[11] Hu Sean, H., and Xiaolin Zhong, "Hypersonic Boundary Layer Stability Over Blunt Leading Edges with Bow-Shock Effects," 36th Aerospace Sciences Meeting, Reno, NV, AIAA Paper 98-0433, 12–15 Jan. 1998.

[12] Chrusciel, G. T., "Analysis of Re-Entry Vehicle Behavior during Boundary-Layer Transition," *AIAA Journal*, Vol. 13, No. 2, Feb. 1975, pp. 154–159.

[13] Kirsch, A. A., "A Proposed Dynamic Stability Solution," AIAA Paper 1973-180, 1973.

[14] Martellucci, A., and Neff, R. S., "Influence of Asymmetric Transition on Re-Entry Vehicle Characteristics," *Journal of Spacecraft and Rockets*, Vol. 8, No. 5, May 1971, pp. 476–482.

[15] Martellucci, A., "Asymmetric Transition Effects on the Stability and Motion History of a Slender Vehicle," Space and Missile Systems Organization, TR-70-141, Los Angeles, Jan. 1970.

[16] Stetson, K. F., "Mach 6 Experiments of Transition on a Cone at Angle of Attack," *Journal of Spacecraft and Rockets*, Vol. 19, No. 5, Sept. 1982, p. 397.

[17] Holden, M. S., " Studies of Boundary Layer Transition and Surface Roughness Effects in Hypersonic Flow," Calspan–Univ. at Buffalo Research Center, Buffalo, NY, Oct. 1983.

[18] Holden, M. S., Bower, D. R., and Chadwick, K. M., "Measurements of Boundary Layer Transition on Cones at Angle of Attack for Mach Numbers from 11 to 13," Calspan–Univ. at Buffalo Research Center, Buffalo, NY, May 1994.

[19] Martellucci, A., "An Experimental Investigation of Boundary Layer Transition on a Cone at Angle of Attack," U.S. Air Force Space and Missile System Organization Rept. SAMSO-TR-69-383, Sept. 1969.

[20] Ericcson, L. E., " Transition Effects on Slender Vehicle Stability and Trim Characteristics," *Journal of Spacecraft and Rockets*, Vol. 11, Jan. 1974, pp. 3–11.

[21] Muir, J. F., and Trujillo, A.A., "Experimental Investigation of the Effects of Nose Bluntness, Free Stream Unit Reynolds Number, and Angle of Attack on Cone Boundary Layer Transition at a Mach Number of 6," AIAA Paper 72-216, Jan. 1972.

[22] Stetson, K. F., and Rushton, G. H., "Shock Tunnel Investigation of Boundary Layer Transition at $M = 5.5$," *AIAA Journal*, Vol. 5, pp. 899–906, May 1967.

[23] Holden, M., "Experimental Studies of the Effects of Asymmetric Characteristics of Hypersonic Blunted Slender Cones," AIAA Paper 85-0325, 14–17 Jan. 1985.

[24] Platus, D. H., "Dispersion of Spinning Missile Due to Lift Non-Averaging," *AIAA Journal*, Vol. 15, July 1977, pp. 905–915.

[25] Murphy, C. H., and Bradley, J. W., "Jump Due to Aerodynamic Asymmetry of a Missile with Varying Roll Rate," U.S. Army Research Labs., Rept. 1077, Adelphia, MD, May 1959.

[26] Platus, D. H., "Ballistic Re-Entry Vehicle Flight Dynamics," *Journal of Guidance and Control*, Vol. 5, No. 1, Jan. 1982, p. 4.

[27] Todisco, A., Reeves, B., Siegelman, D., and Mascola, R., "Boundary Layer Transition on Blunt Axi-Symmetric Nosetip Induced by Single and Multiple Craters," *AIAA Journal*, Vol. 21, No. 7, July 1983, pp. 939–940.

[28] Demetriades, A., Laderman, A., Von Seggern, L., Hopkins, T., and Donaldson, J., "Effects of Mass Addition on the Boundary Layer of a Hemisphere at Mach 6," *Journal of Spacecraft and Rockets*, Vol. 13, No. 8, 1976, pp. 508–509.

[29] Batt, R. G., and Legner, H. L., "A Review of Roughness-Induced Nosetip Transition," *AIAA Journal*, Vol. 21, No. 1, 1983, p. 7.

[30] Bartlett, E. P., Abbett, M. J., Nicolet, W. E., and Moyer, C. B., "Improved Heat-Shield Design Procedures for Manned Entry Systems," NASA CR-108689, June 1970; also Aerotherm Corp., Rept. 70-15, Mountain View, CA, June 1970.

R. Kimmel
Associate Editor